Large-eddy simulations with wall models

By W. Cabot

1. Motivation and objectives

The near-wall viscous and buffer regions of wall-bounded flows generally require a large expenditure of computational resources to be resolved adequately, even in large-eddy simulation (LES). Often as much as 50% of the grid points in a computational domain are devoted to these regions. The dense grids that this implies also generally require small time steps for numerical stability and/or accuracy. It is commonly assumed that the inner wall layers are near equilibrium, so that the standard logarithmic law can be applied as the boundary condition for the wall stress well away from the wall, for example, in the logarithmic region, obviating the need to expend large amounts of grid points and computational time in this region. This approach is commonly employed in LES of planetary boundary layers (e.g., Mason, 1989; Schmidt & Schumann, 1989), and it has also been used for some simple engineering flows (e.g., Piomelli *et al.*, 1989; Arnal & Friedrich, 1993).

In order to calculate accurately a wall-bounded flow with coarse wall resolution, one requires the wall stress as a boundary condition. The incompressible Navier-Stokes equation is

$$\frac{\partial \mathbf{u}}{\partial t} = -\nabla p + \nabla \cdot \boldsymbol{\tau}\,, \quad \boldsymbol{\tau} = -\mathbf{u}\mathbf{u} + \nu \nabla \mathbf{u}\,, \tag{1}$$

in which $\mathbf{u}$ is the velocity, p is the pressure, $\boldsymbol{\tau}$ is the stress, and ν is the molecular viscosity. In a simulation with an unresolved wall, the wall-normal (y) derivative of the stress for tangential (x, z) velocity components,

$$\frac{\partial}{\partial y}\left(-u_i v + \nu \frac{\partial u_i}{\partial y}\right)\,, \quad i = 1, 3\,, \tag{2}$$

cannot be accurately calculated by applying the usual no-slip condition, $\mathbf{u} = 0$, instead requiring the specification of the wall stress

$$\tau_{i2w} = \nu \left.\frac{\partial u_i}{\partial y}\right|_{y=0}\,, \quad i = 1, 3\,. \tag{3}$$

Thus, an adequate model of τ_{i2w} based on outer flow quantities is desired. Asymptotic matching of inner and outer regions in steady, ensemble-averaged, equilibrium flow yields the log-law relation between wall stress and outer mean velocity. However, for the purposes of LES, wall stress models are needed with some degree of time and space dependence. Because the near-wall layer is typically very thin with respect to horizontal scales, boundary layer assumptions may be valid, perhaps even

on horizontal grid scales used in LES, and it may be possible to use simpler boundary layer equations to model the near-wall region and at the same time retain more flexibility in handling flows with widely varying pressure gradients.

The goal of this work is to determine the extent to which equilibrium and boundary layer assumptions are valid in the near-wall regions, to develop models for the inner layer based on such assumptions, and to test these modeling ideas in some relatively simple flows with different pressure gradients, such as channel flow and flow over a backward-facing step. Ultimately, models that perform adequately in these situations will be applied to more complex flow configurations, such as an airfoil.

2. Accomplishments

An examination of momentum balance at different horizontal scales, and correlations between the measured wall stress and some outer flow quantities, have been performed from a direct numerical simulation (DNS) database for channel flow. Because wall stresses need to be predicted in flows with different pressure gradients and in separated flow, models based on the log law and boundary layer equations have been tested both in channel and backward-facing step flows.

2.1 Momentum balance in channel flow

Near-wall data has been examined from a channel flow DNS (J. Kim, personal communication; Kim, Moin & Moser, 1987) with a friction Reynolds number $Re_\tau = 395$ ($Re_\tau \equiv u_\tau \delta/\nu$, where δ is the channel half-width, $u_\tau \equiv |\nu dU/dy|^{1/2}$ is the friction speed, and U is the mean streamwise velocity). Horizontal averages of flow quantities were taken over different scales, from the scale of the entire plane down to scales comparable to expected LES resolutions (a factor of 16 smaller in each direction, or $\Delta x^+ \times \Delta z^+ \approx 160 \times 80$ in wall units scaled by ν/u_τ). The streamwise momentum balance was constructed by integration over volumes with these horizontal dimensions from the wall to a height $y^+ \approx 80$:

$$\left\langle \frac{\partial u}{\partial t} + \frac{\partial u^2}{\partial x} + \frac{\partial uw}{\partial z} + \frac{\partial p'}{\partial x} \right\rangle = -\frac{dP}{dx} + \left\langle \nabla\cdot(\nu\nabla u) - \frac{\partial uv}{\partial y} \right\rangle , \qquad (4)$$

where $\langle \cdots \rangle$ denotes a volume average, and dP/dx is the mean pressure gradient. The results shows that the advection and fluctuating pressure gradient terms on the left-hand side of (4), while small compared to the other terms when averaged over the entire plane, are more than an order of magnitude larger at LES scales. This suggests that momentum balance is dominated by a nearly inviscid balance between advection and pressure gradients at LES scales, casting doubt on the local validity of models, such as the log law, based on a balance between terms on the right-hand side of (4) (J. Jiménez, personal communication).

Correlations between the wall stress τ_{12w} and the mean streamwise velocity at $y^+ \approx 40$ are small but significant (50% at LES scales). Figure 1 shows a scatter plot of the deviation from the mean of actual wall stress versus that predicted from a logarithmic law with the (nearly zero) mean pressure gradient in the channel at

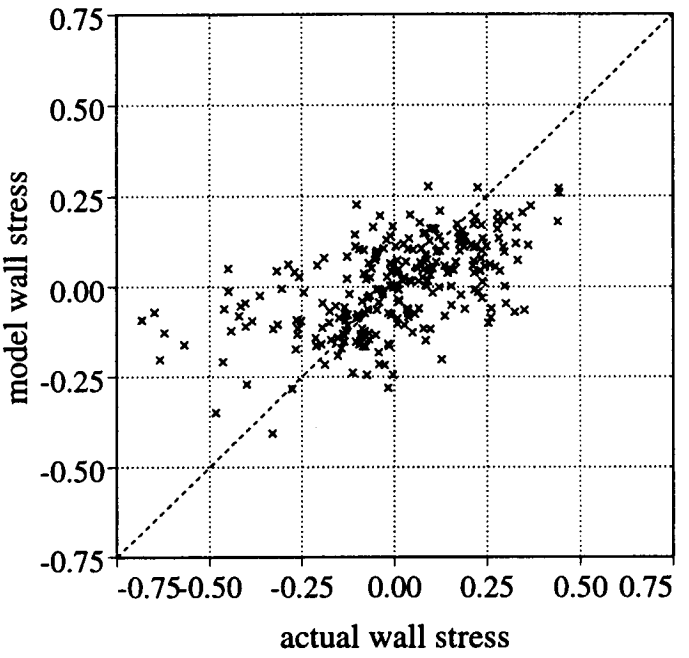

FIGURE 1. Deviation from the mean of actual wall stress from DNS channel flow data ($Re_\tau = 395$) compared with that predicted from the log law model applied at $y^+ \approx 40$. The flow is averaged horizontally on typical LES scales ($\Delta x^+ \times \Delta z^+ \approx 160 \times 80$). The linear diagonal denotes a perfect local correlation.

$y^+ \approx 40$. There is a noticeable linear correlation for values of wall stress near the mean, with larger deviations in high-stress regions. (The nature of the high-stress events has yet to be explored.) On the other hand, the correlation of wall stress to the large, instantaneous, fluctuating pressure gradients is found to be practically nil (only a few percent). Corresponding analyses need to be performed with DNS and LES databases for flow over a backward-facing step (Le & Moin, 1993; Akselvoll & Moin, 1995), which contain a large adverse pressure gradient and separated flow.

2.2 Boundary layer wall models in channel flow

Wall models have been tested in a second-order, central finite difference (FD2) channel code on a staggered mesh with a third-order Runge-Kutta (RK3) time advancement (Akselvoll & Moin, 1995), in which the wall stress boundary conditions are easily implemented. These wall models have been based on the Johnson-King (1985) boundary layer model, which is fairly simple and has had good success in Reynolds-averaged Navier-Stokes (RANS) models of separated flow (Menter, 1991).

A channel flow with a target $Re_\tau = 1030$ was simulated using an outer mesh with the near-wall points for horizontal velocity placed at a matching height $y_m^+ = 32$ or 64. Embedded in the outer mesh is a fine sublayer mesh from the wall to the matching height. The outer mesh technically extends to the walls, but only the

$v = 0$ and $\partial p/\partial y = 0$ boundary conditions are used. Both outer and inner meshes are usually stretched with a hyperbolic tangent mapping. The outer mesh uses 33 wall-normal nodes, and the sublayers uses 21 nodes at each wall. The horizontal domain size is $\Delta x \times \Delta z = 2\pi\delta \times \pi\delta$. Initially, a horizontal mesh of 32×32 was used for both outer and sublayer regions, but it was found that much better results were obtained with a finer 64×64 mesh for the outer region; on the other hand, the mean velocity and rms statistics were found to be insensitive to whether the sublayer mesh was 32×32 or 64×64 ($\Delta x^+ \times \Delta z^+ \approx 200 \times 100$ or 100×50). It was also found that results from the FD2-RK3 code were sensitive to the time step for convective CFL numbers exceeding about 0.5, perhaps due to inaccuracies in implicit terms (cf. Choi & Moin, 1994). In the results presented here, the convective CFL number was kept around 0.6.

Model JK0. The lowest level model for the wall stress is obtained at each horizontal position in the near-wall sublayer (independent of other horizontal locations) from the solution of the ordinary differential equation

$$\frac{d}{dy}(\nu + \nu_t)\frac{dU_i}{dy} = \frac{dP}{dx_i}, \quad i = 1,3, \tag{5}$$

where U_i are the horizontal velocity components in the sublayer, dP/dx_i is the constant mean pressure gradient, and

$$\nu_t = \kappa u_s y_w D^2, \quad D = 1 - \exp(-u_d y_w / A\nu), \tag{6}$$

resembles the eddy viscosity in the Johnson-King (JK) model for the inner regions. Here, though, the scale speeds u_s and u_d are replaced by the friction speed u_τ; y_w is the distance from the wall, κ is the von Kármán constant, and A is a damping-function constant taken to be 19, which gives the best fit to the standard log law in this case (lower values were used by Johnson & King and Menter). The boundary conditions for (5) are $U_i = 0$ at the walls and U_i equal to the horizontal velocity in the outer mesh at the first grid point above the wall. The wall-normal derivative of U_i at the wall yields the wall stress τ_{i2w} used in the outer flow. Eq. (5) is solved by using the same FD2 discretization used in the main code and performing an inversion of the resulting tridiagonal matrix. The solution of (5) is just a smooth blend of the viscous and logarithmic functions and, for the channel, is generally equivalent an instantaneous log law. Because one can consider expressions like (5) to be valid only in some average sense, both in space and time, a running time-average of the matching velocity over about an eddy turnover time is employed.

Model JK0a. The next level of model tests the influence of large advective and instantaneous pressure gradient terms:

$$\frac{\partial}{\partial y}(\nu + \nu_t)\frac{\partial U_i}{\partial y} = \frac{\partial U_i}{\partial t} + \nabla\cdot(U_i \mathbf{U}) + \frac{\partial p}{\partial x_i}, \quad i = 1,3, \tag{7}$$

where U_i are the horizontal velocity components in the sublayer, as in (5). The eddy viscosity is given by (6) and, as in the JK0 model above, uses $u_s = u_d = u_\tau$.

The solutions of (7) at different horizontal locations are now coupled through the divergence term, which is calculated from differences of velocity components on the sublayer mesh. The wall normal velocity $V \equiv U_2$ is calculated locally at each sublayer grid point from differences of the horizontal velocity components using the continuity equation,

$$V = -\int_0^y \frac{\partial U_i}{\partial x_i} dy \,. \tag{8}$$

The usual boundary layer assumption that $\partial p/\partial y = 0$ is used; hence the pressure gradient in (7) for a given horizontal location is set to be constant at all wall-normal locations in the sublayer, using the value in the outer flow at the matching point. A running time average of the pressure gradient is actually used to smooth the wall model. Eq. (7) is discretized and integrated with the same FD2-RK3 scheme used in the main code.

Model JK1. The actual JK model for the inner regions uses velocity scales (u_s and u_d) in the eddy viscosity expression (6) that are melds of u_τ and u_m, where u_m is the square root of the maximum Reynolds stress ($-\overline{uv}$) that occurs at a distance $y_{\max}$ above the wall:

$$u_s = (1-\gamma)u_\tau + \gamma u_m \,, \quad \gamma = \tanh(y_w/\ell) \,, \quad \ell = u_\tau y_{\max}/(u_\tau + u_m) \,, \tag{9a}$$

$$u_d = \max(u_m, u_\tau) \,. \tag{9b}$$

Model JK1 calculates U_i from (5), but uses (9) to compute the eddy viscosity in (6). In RANS models, u_m and $y_{\max}$ are determined from the solution of an ODE. In LES, the maximum of the stress can in principle be found on the fly at a given horizontal position from values of the Reynolds stress in the sublayer and overlying outer layer. In practice, this is much more difficult to accomplish with any great accuracy, because instantaneous values of the stress along a vertical line fluctuate wildly in space and time. Again, a running time average must be used, along with some local spatial filtering, in order to smooth the signal to a useful level; then a search routine is employed to find the first local maximum of averaged stress moving away from the wall at a given horizontal location. Because this is a rather costly and cumbersome procedure to employ in LES, its benefits must be shown to be substantial to justify its use.

The computational overheads of the above wall models were about 10, 20, and 30% of total cost, respectively; however, the number of interior points was halved and the time step used was 3 times larger than in a regular, resolved LES, so that a savings factor of about 5 was realized.

The mean streamwise velocities that are obtained using these wall models for channel flow are shown in Fig. 2a in comparison with the experimental data (Hussain & Reynolds, 1975) and with a LES (Cabot, 1994) for the same parameters with the same code without wall models (using 65 wall-normal nodes with about the same interior resolution as the LES with wall models and a 64×64 horizontal mesh). It is seen that there is little difference between the results for different wall models in channel flow, suggesting that a simple instantaneous log law provides

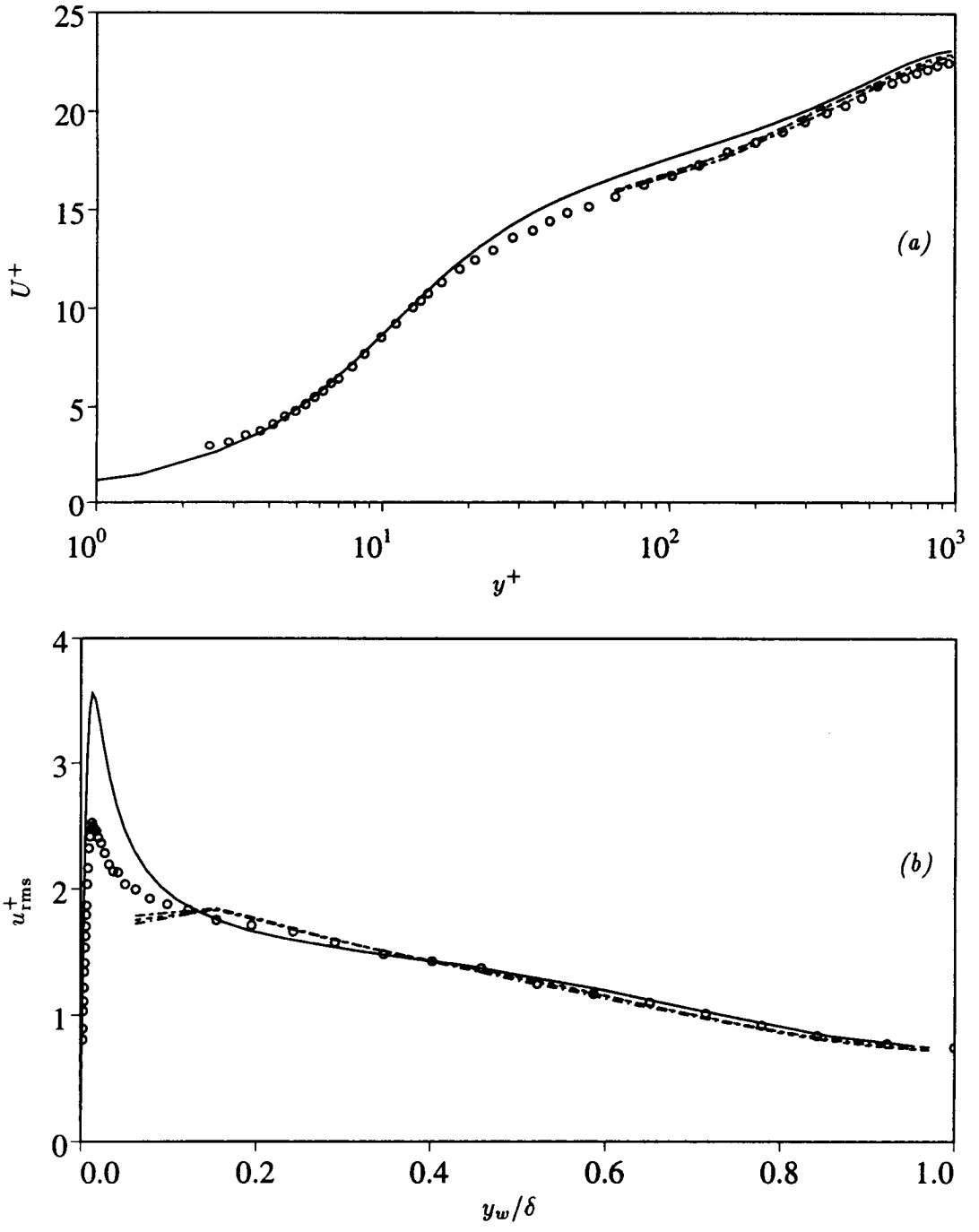

FIGURE 2. Mean streamwise (a) velocity and (b) velocity fluctuation intensities in channel flow for LES with different wall models (---- JK0, —·— JK0a, —·— JK1), compared with a full LES (—— , Cabot, 1994) and experimental data (o o o , Hussain & Reynolds, 1975).

an adequate, cost-effective wall model in this case. The results for U in the outer region are in generally fair agreement with the experimental data and full LES. The streamwise velocity fluctuation intensities ($u_{\rm rms}$) are shown in Fig. 2b and also show fair agreement with experimental and full LES results, with some discrepancies near the matching point. Note that there is a large disagreement between the full LES results and experimental data in the near-wall region where $u_{\rm rms}$ peaks ($y^+ \leq 50$). The results were insensitive to whether the matching point was at $y^+ = 32$ or 64.

2.3 Boundary layer wall models behind a backward-facing step

Wall models JK0 and JK0a have also been implemented in the LES of flow over a backward-facing step using the same FD2-RK3 scheme used for the channel (Akselvoll & Moin, 1995). The flow has a Reynolds number of 28,000 based on the centerline velocity of the inlet flow and the step height h. There is a long inlet section $10h$ long, $4h$ high, and $2h$ wide on a $100 \times 65 \times 96$ mesh followed by a $20h \times 5h \times 2h$ outlet section on a $146 \times 97 \times 96$ mesh; both x and y coordinates are stretched. The wall model is implemented only along the bottom wall behind the step for test purposes, with a $74 \times 33 \times 48$ sublayer mesh embedded below $y \approx 0.073$ or $y^+ \approx 60$ at the outlet. No account is taken of the geometry of the corner behind the backstep, where there is a weak recirculation zone, but this inaccuracy is not expected to affect the bulk of the flow very much. Because only about 10% of the grid points are removed from the main calculation and time steps can only be increased by about 30%, little computational saving is gained from the wall model in this case.

There is a strong adverse pressure gradient between about $3h$ and $7h$ behind the step and a concomitant separation bubble in this region. Figure 3 shows the near-wall ($y/h \approx 0.10$) streamwise pressure gradient from Akselvoll & Moin's (1995) LES, averaged over time and span; the mean wall-normal gradient of streamwise velocity (proportional to the wall stress) is also shown. The assumption that there is no wall-normal variation in pressure gradient is found to be good for the most part, except in a few regions associated with relatively rapid wall-normal velocities in the reattachment region around $x/h = 5$–8. Preliminary results from the application of the JK0 wall model (which includes no pressure gradient or advection terms) show an underprediction of the level of reversed wall flow (Fig. 3); the recovery region around $x/h = 10$ is also not predicted very well, nor is the recirculation region near the step. The level of the post-recovery region near the outlet is predicted better; but this region is in fact similar to channel flow or a zero-pressure-gradient boundary layer, in which this model was seen to give good results (§2.2). Longer runs (currently in progress) are needed to see how the flow adjusts itself further, and if the resulting statistically steady flow is predicted adequately.

The large pressure gradient and advection terms in Eq. (7) are probably required to obtain better agreement. For instance, if the streamwise pressure gradient integrated over the thickness of the sublayer y_m, which is about $y_m \partial p/\partial x$, is comparable to $\tau_{12w} = \nu \partial U/\partial y|_w$, then it can be expected to significantly modify the structure of the boundary layer and the wall stress itself. In Fig. 3 the streamwise pressure

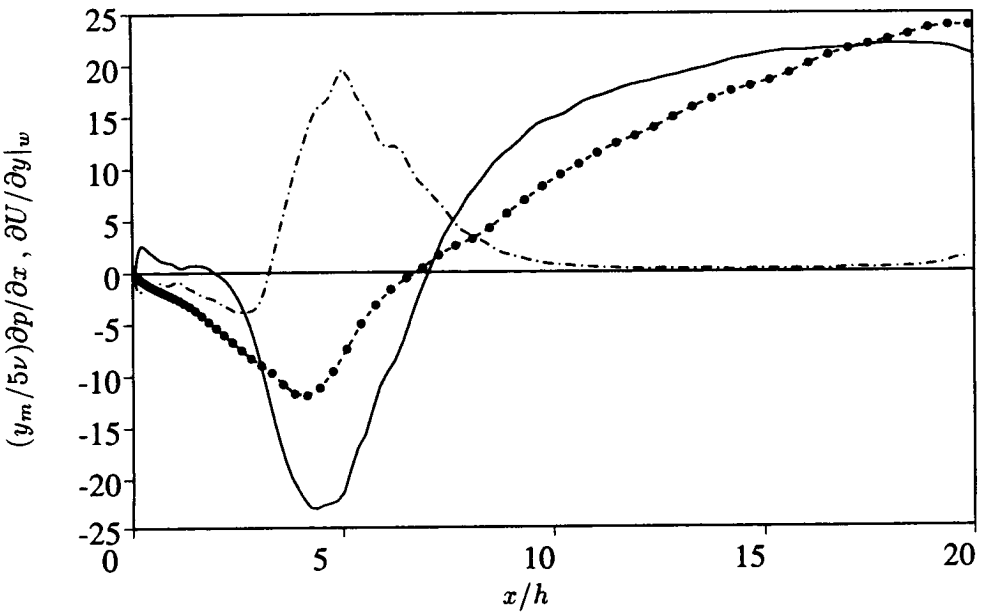

FIGURE 3. Mean wall-normal gradient of the streamwise velocity at the bottom wall $\partial U/\partial y|_w$ (———) and mean streamwise pressure gradient near the bottom wall $\partial p/\partial x$ (—·—) behind a backward-facing step from the LES of Akselvoll & Moin (1995). The pressure gradient is scaled by $y_m/5\nu$, where y_m is the thickness of the sublayer used in wall model calculations. Preliminary values of mean $\partial U/\partial y|_w$ predicted with the JK0 wall model are also shown (• • •).

gradient multiplied by $y_m/5\nu$ is seen to be comparable to $\partial U/\partial y|_w$ in the separation and recirculation regions, and it is likely to have an important effect there. Of course, the effect of pressure gradient term will be mitigated to a large degree by the advection terms (mostly $\partial U^2/\partial x$) in the outer part of the sublayer, but these terms vanish very near the wall, while the pressure gradient does not.

Application of the JK0a model, with the addition of large pressure gradient and advection terms, shows a much better initial agreement in the reverse flow region, although the recovery region around $x/h = 10$ is still not well predicted. The region around $x/h = 5$ near the head of the separation bubble in the reattachment zone, characterized by downflows that are strong in comparison with horizontal flow, has led to numerical instability in the sublayer calculation. The cause of this is still not known, but it appears to be associated with very large advection terms $\partial(U_iV)/\partial y$ at locations of rapid downflow. These are also regions where the assumption of constant horizontal pressure gradients breaks down and the boundary layer equations are known to be invalid.

3. Future plans

Some fundamental tests need to be performed on backward-facing step flow fields near the bottom wall, such as the momentum balance at different scales that was

performed for channel flow (§2.1). DNS and LES fields will be studied to attempt to determine, for example, how the changes in pressure gradient affect in detail the wall stress and what terms in the momentum equation are most important in the regions of strong downflow at the head of the separation bubble.

LES with the simple JK0 wall model (essentially the smooth meld of the log law and viscous law) will be run over long times to statistical equilibrium to get a fair assessment of that model's performance. The same model with advection and running time-averaged pressure terms (JK0a) will also be run to longer times if the present numerical instability can be cured. An attempt will also be made to implement the JK1 wall model in the backward-facing step flow, which requires a determination of the maximal shear stress (averaged in some sense) above the wall in order to determine a model velocity scale. Search routines like that used in channel flow, and perhaps a curve fitting scheme applied to the shear stress profiles, will be tried; however, there is always some arbitrariness in these approaches. Alternative, more easily determined, and better quantified velocity scales will also be considered.

REFERENCES

AKSELVOLL, K., & MOIN, P. 1995 Large eddy simulation of turbulent confined coannular jets and turbulent flow over a backward facing step. Dept. of Mech. Eng. Tech. Rep. **TF-63**, Stanford Univ.

ARNAL, M., & FRIEDRICH, R. 1993 Large-eddy simulation of a turbulent flow with separation. In *Turbulent Shear Flows 8*, ed. by F. Durst *et al.*, Springer-Verlag (Berlin), pp. 169–187.

CABOT, W. 1994 Local dynamic models in channel flow. In *Annual Research Briefs 1994*, Center for Turbulence Research, NASA Ames/Stanford Univ., 143–159.

CHOI, H., & MOIN, P. 1994 Effects of the computational time step on numerical solutions of turbulent flow. *J. Comp. Phys.* **113,** 1–4.

HUSSAIN, A. K. M. F., & REYNOLDS, W. C. 1970 The mechanics of a perturbation wave in turbulent shear flow. Dept. of Mech. Eng. Tech. Rep. **FM-6**, Stanford Univ.

JOHNSON, D. A., & KING, L. S. 1985 A mathematically simple turbulence closure model for attached and separated turbulent boundary layers. *AIAA J.* **23,** 1684–1692.

KIM, J., MOIN, P., & MOSER, R. 1987 Turbulence statistics in fully developed channel flow at low Reynolds number. *J. Fluid Mech.* **177,** 133–166.

LE, H., & MOIN, P. 1993 Direct numerical simulation of turbulent flow over a backward-facing step. In *Annual Research Briefs 1992*, Center for Turbulence Research, NASA Ames/Stanford Univ., 161–173.

MASON, P. J. 1989 Large-eddy simulation of the convective atmospheric boundary layer. *J. Atmos. Sci.* **46,** 1492–1516.

MENTER, F. R. 1991 Performance of popular turbulence models for attached and separated adverse pressure gradient flows. *AIAA Paper.* **91-1784.**

PIOMELLI, U., FERZIGER, J., MOIN, P., & KIM, J. 1989 New approximate boundary conditions for large eddy simulations of wall-bounded flows. *Phys. Fluids A.* **1,** 1061–1068.

SCHMIDT, H., & SCHUMANN, U. 1989 Coherent structure of the convective boundary layer derived from large-eddy simulations. *J. Fluid Mech.* **200,** 511–562.